Catalytic chemical vapor deposition synthesis of single- and double-walled carbon nanotubes from α-(Al1–xFex)2O3 powders and self-supported foams

Valdirene Gonzaga de Resende, Eddy de Grave, Anne Cordier, Alicia Weibel, Alain Peigney, Christophe Laurent

Catalytic chemical vapor deposition synthesis of single- and double-walled carbon nanotubes from α-$(Al_{1-x}Fe_x)_2O_3$ powders and self-supported foams

Valdirene G. de Resende[a,b,], Eddy De Grave[a], Anne Cordier[b], Alicia Weibel[b], Alain Peigney[b], Christophe Laurent[b]*

[a]*Department of Subatomic and Radiation Physics, University of Ghent, Proeftuinstraat 86, B-9000 Gent, Belgium*
[b]*CIRIMAT UMR CNRS 5085/LCMIE, Centre Interuniversitaire de Recherche et d'Ingénierie des Matériaux, Université Paul-Sabatier, 31062 Toulouse Cedex 9, France*

A B S T R A C T

An investigation of the potential interest of α-alumina–hematite foams, as opposed to powders, as starting materials for the synthesis of carbon nanotubes (CNTs) by catalytic chemical vapor deposition method was performed. The oxide powders and foams as well as the corresponding CNT–Fe–Al_2O_3 composite powders and foams are studied by X-ray diffraction, specific surface area measurements, electron microscopy, Raman spectroscopy and Mössbauer spectroscopy. The latter technique revealed that four components (corresponding to α-Fe, Fe_3C, γ-Fe-C and Fe^{3+}) were present in the Mössbauer spectra of the composite powders, and that an additional sextet, possibly due to an $Fe_{1-y}C_y$ alloy, is also present in the Mössbauer spectra of the composite foams. Contrary to some expectations, using foams do not lead to an easier reduction and thus to the formation of more α-Fe, Fe_3C and/or γ-Fe–C potentially active particles for the formation of CNTs, and hence to no gain in the quantity of CNTs. However, using foams as starting materials strongly favors the selectivity of the method towards SWCNTs (60% SWCNTs and 40% DWCNTs) compared to what is obtained using powders (5% SWCNTs, 65% DWCNTs and 30% MWCNTs).

1. Introduction

The synthesis of carbon nanotubes (CNTs) by catalytic chemical vapor deposition (CCVD) is based on the catalytic decomposition of carbonaceous gases such as CH_4 on transition metal (usually Fe or Co) nanoparticles. The nanoparticles are either supported by a substrate, or held in suspension in the gas stream. A critical survey of the bibliography [1] revealed that many different CCVD routes can succeed provided all parameters related to the metal source are adapted to all parameters related to the carbon source, at the appropriate synthesis temperature. Indeed, the critical step is the formation of metal nanoparticles, which must have a size (0.4–5 nm) adequate for the formation of single-wall CNTs (SWCNTs) and double-wall CNTs (DWCNTs) [2,3] at a temperature (usually in the range 600–1100 °C) making possible the catalytic (as opposed to thermal) decomposition of the carbonaceous gas.

One method [4], ensuring that the metal particles do not grow too much, involves the reduction in H_2–CH_4 of

* *Corresponding author:* Address: Department of Subatomic and Radiation Physics, University of Ghent, Proeftuinstraat 86, B-9000 Gent, Belgium. Fax: +32 9 264 6697.
E-mail address: valdirene.gonzaga@ugent.be (V.G. de Resende).

doi:10.1016/j.carbon.2008.10.027

alumina–hematite solid solutions, first producing nanometric Fe particles that are active for the decomposition of CH_4, thus producing CNT–Fe–Al_2O_3 composite powders. The influence of the characteristics of the solid solutions upon the synthesis of CNTs has been the subject of intensive research. In particular, in order to increase the quantity of CNTs, it is desirable that there are more Fe nanoparticles on the surface of the oxide grains. Increasing the geometrical surface area by a grinding which decreases the grain size of the starting powder of alumina–hematite solid solution was not found [5] to be useful, possibly because of the much higher packing of the ground powder. When using the high-specific-surface-area amorphous or transition solid solutions prepared from the mixed-oxalate decomposition and calcination, it was found [6] that some undesirable carbon species are entrapped within the Al_2O_3 grains upon the crystallization into the corundum (α) form which occurs during the H_2–CH_4 reduction step. Thus, the aim of this paper is to investigate a new way to prepare α-alumina–hematite starting materials. This will involve the preparation of self-supported foams. The advantage of the shaping into to a foam, as opposed to a powder, is that the porous oxide solid solution presents a very low packing, which should permit firstly to obtain more active surface area and therefore catalyst nanoparticles and secondly to maintain free space that will allow a good diffusion of CH_4. This route has given promising results when applied to catalytic materials based on (Mg,Co)Al_2O_4 [7] and (Mg,Co,Mo)O [8]. CNTs–Fe–Al_2O_3 composite powders and foams will be studied by electron microscopy, Raman spectroscopy and Mössbauer spectroscopy.

2. Experimental

2.1. Preparation of powders and self-supported foams

α-$(Al_{1-x}Fe_x)_2O_3$ (corundum) powders (x = 0.02, 0.05, 0.07, 0.10) were prepared by decomposition and calcination of the Al/Fe oxinate precursors whose preparation is detailed elsewhere [9]. The powders were code-named as PX, where X represents the iron content (2, 5, 7 and 10 cat.%) in the solid solution.

About 3 g of each α-$(Al_{1-x}Fe_x)_2O_3$ powder was mixed with 0.045 g of dispersant (BEYCOSTAT C213, CECA France), which represents 1 mg of dispersant/m^2 of powder, diluted in about 10 mL of ethanol. The mixture was kept under magnetic stirring for about 10 min for homogenization. The so-obtained dispersant-powder mixture was attrition-milled (2000 rpm, 3 h) using a Nylon vessel and rotor, and alumina balls (200–300 μm in diameter). The ratio between the powder volume and the volume of the balls was 0.5. After attrition milling, the powder was separated from the alumina balls by rinsing in ethanol and filtering. The composition of the resulting slurry was adjusted to about 35 wt% dispersant-powder mixture and 65 wt% ethanol. A polyurethane foam (80 pores per inch, $60 \times 30 \times 20$ mm^3) was impregnated with the slurry. The impregnated foam was mechanically pressed several times in order to eliminate the excess slurry. It was then dried overnight at room temperature and calcinated in air (600 °C, 150 °C/h, 60 min) in order to burn all organics, producing the self-supported α-$(Al_{1-x}Fe_x)_2O_3$ foams. These foams were code-named as FX, after the corresponding powder PX. Note that only three foams were prepared (F2, F5 and F7).

2.2. Synthesis of carbon nanotubes

The solid solution powders and foams were reduced in a H_2–CH_4 (20 mol% CH_4) gas mixture in a silica reactor (inner diameter 56 mm, length of the heating zone 200 mm). The heating and the cooling rate to the desired temperature (1025 °C) and back to room temperature was 5 °C/min. No dwell time was applied at 1025 °C. The flowing gas was dried on P_2O_5 and its composition was regulated by mass-flow controllers. The total flow rate was 15 L/h. The so-obtained CNTs–Fe–Al_2O_3 composite powders and foams are code-named as PXR and FXR, respectively.

2.3. Characterization

X-ray diffraction (XRD) patterns were recorded in the range 10–70° (2θ) with a Bruker D4 Endeavor diffractrometer operating with Cu Kα radiation. Counts were registered every 0.02° (2θ). The specific surface area of the oxide powders and foams was measured by the BET method (Micrometrics Flow Sorb II 2300) using nitrogen adsorption at liquid nitrogen temperature. This instrument gives a value from one point (i.e. one adsorbate pressure) and requires calibration. The reproducibility of the results is in the ±3% range. Mössbauer spectra at room temperature (295 K) and at 15 K were collected using spectrometers operating at constant acceleration mode with triangular reference signals. ^{57}Co(Rh) sources were used. All Mössbauer spectra were analyzed in terms of model-independent distributions of hyperfine parameter values and numerical data quoted hereafter refer to maximum-probability values [10]. Isomer shifts are referenced with respect to α-Fe at room temperature. The carbon content (C_n) in the composite powders and foams was measured by the flash combustion method with an accuracy of ±2%. Raman spectra were recorded using a LabRAM 800 Jobin–Yvon spectrometer (632.82 nm) and were averaged on three spectra. The powders and foams were observed by field-emission-gun scanning electron microscopy SEM (FEG–SEM, JEOL JSM 6700F). The observations were performed with a tension of 5 kV and a work distance between 4.0 and 6.2 mm. Composite specimens were plated with Pt before FEG–SEM observations. High-resolution transmission electron microscopy (HRTEM) was performed with a JEOL JEM 2100F microscope operated at 200 kV. The samples were slightly sonicated in ethanol, and a drop of the suspension was deposited onto a holey carbon grid.

3. Results and discussion

3.1. Oxide powders and foams

The XRD patterns of the PX powders (not shown) show peaks characteristic of well-crystallized corundum solid solution. For P10, however, several weak additional lines corresponding to hematite (α-Fe_2O_3) are observed. This reveals that for this

Table 1 – Hyperfine parameters at room temperature for the α-$(Al_{1-x}Fe_x)_2O_3$ powders [9].

Sample	D1			D2			Sg		S1			
	ΔE_Q (mm/s)	δ[a] (mm/s)	RA (%)	ΔE_Q (mm/s)	δ[a] (mm/s)	RA (%)	δ (mm/s)	RA (%)	B_{hf} (T)	$2\varepsilon_Q$ (mm/s)	δ (mm/s)	RA (%)
P2	0.54	0.30	63	1.18	0.30	29	0.03	8				
P5	0.53	0.30	85	1.18	0.30	12	0.04	3				
P7	0.54	0.29	88	1.20	0.29	8	0.05[b]	1	49.8	−0.19	0.35	3
P10	0.54	0.29	85	1.20	0.29	7	0.05	0.5	49.8	−0.18	0.37	7.5

B_{hf}, hyperfine field at maximum of the distribution (T); $2\varepsilon_Q$, quadrupole shifts (mm/s); ΔE_Q, quadrupole splitting (mm/s); δ, isomer shifts (mm/s); RA, relative spectral areas (%). The values of isomer shifts are with reference to metallic iron.

a The isomer shifts of D1 and D2 were coupled.

b Fixed parameters.

composition the crystallization of the solid solution into the α phase was followed by some degree of phase partitioning into an alumina-rich corundum phase and a hematite- rich corundum phase. This further infers that the solubility limit of hematite into α-Al_2O_3 for the present synthesis route is below 10 mol%.

The Mössbauer spectra (not shown) of the α-$(Al_{1-x}Fe_x)_2O_3$ powders were studied in detail elsewhere [9]. They are composed of a dominant Fe^{3+} quadrupole doublet with quadrupole splitting $\Delta E_Q \approx 0.54$ mm/s besides two other weaker components, i.e., a singlet and another quadrupole doublet with $\Delta E_Q \approx 1.2$ mm/s. Additionally, the presence of a weak sextet characteristic of α-Fe_2O_3, is observed for samples P7 and P10. The Mössbauer spectra parameters are listed in Table 1 [9]. The dominant doublet was attributed to Fe^{3+} ions substituting for Al^{3+} ions in the corundum structure. The singlet was ascribed, on the basis of its isomer shift value, to extremely small metallic Fe nanoclusters that for some yet unknown reason may have formed within the solid solution grains, which is an unusual result that is discussed elsewhere in great detail [9]. However, the amount of iron involved is very minor (Table 1) and the specimens are nevertheless considered as solid solutions. The isomer shift obtained for the weak doublet (~0.3 mm/s at 295 K) points at an Fe^{3+} species in an octahedral co-ordination. Its high quadrupole splitting ($\Delta E_Q \approx 1.2$ mm/s) implies a strong deformation of the octahedral symmetry of the involved site. As discussed elsewhere [9], these strongly deformed sites could most likely be associated to the presence of the metallic nanoclusters within the solid solution grains. The presence of the weak α-Fe_2O_3 sextet for P7 and P10 indicates that some phase partitioning into an alumina-rich corundum phase and a hematite-rich phase occured during the calcination step. Regarding the self-supported foams, there is no reason to suspect that the process used in the present work produced any change in the distribution of the Fe^{3+} ions.

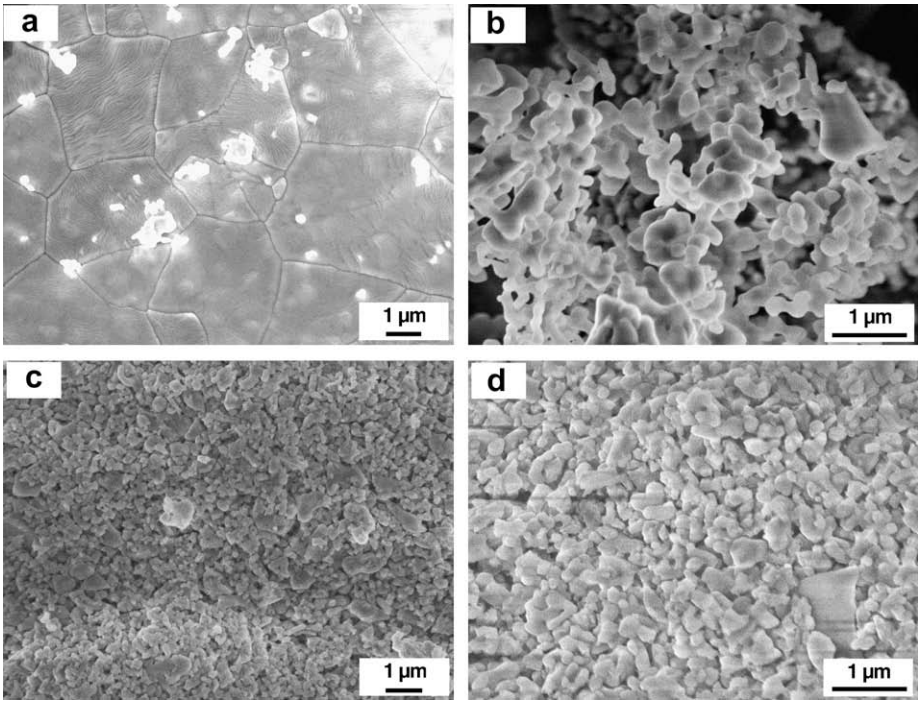

Fig. 1 – Typical FEG–SEM images showing the α-$(Al_{1-x}Fe_x)_2O_3$ powders (a and b) and the walls of the corresponding foams (c and d).

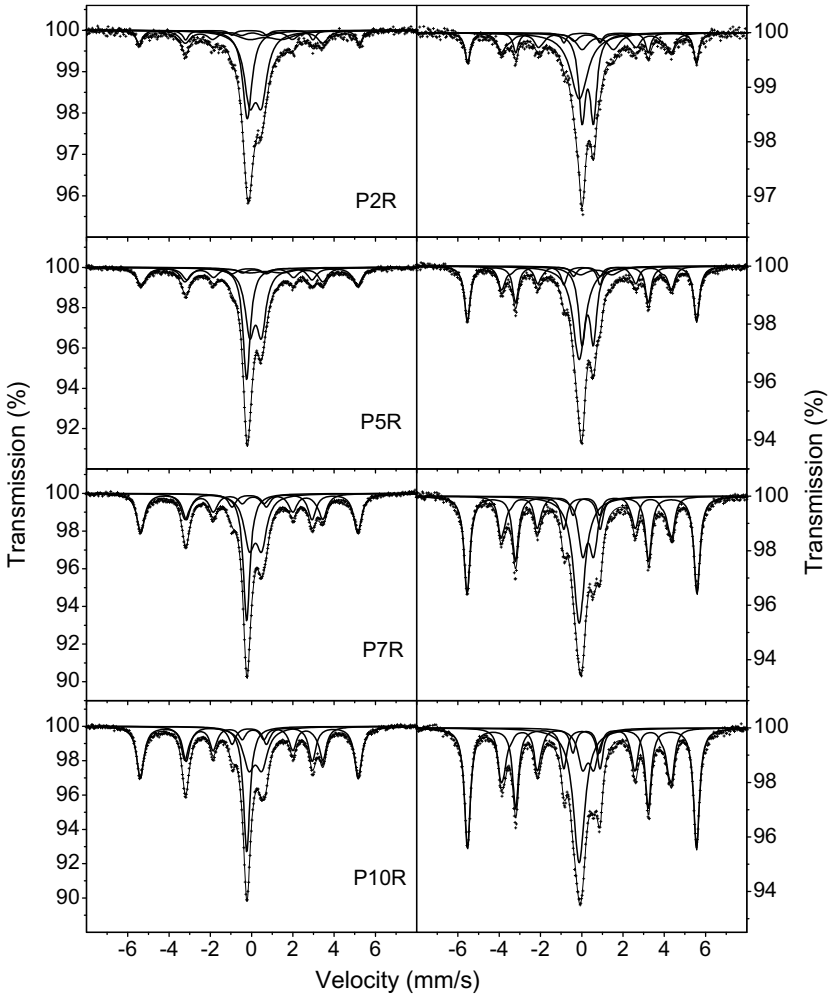

Fig. 2 – MS of the CNTs–Fe–Al_2O_3 powders measured at 295 K (left) and 15 K (right).

Table 2 – Mössbauer results of the CNTs–Fe/alumina powders at 295 K and 15 K. The quadrupole shifts ($2\varepsilon_Q$), quadrupole splitting (ΔE_Q) and isomer shifts (δ) are given in mm/s, the hyperfine fields (B_{hf}) are in T and the relative spectral areas (RA) are given in %. The values of isomer shifts are with reference to metallic iron.

Sample	Fe_3C				α-Fe			γ-Fe–C		$(Al,Fe)_2O_3$		
	B_{hf}	$2\varepsilon_Q$	δ	RA	B_{hf}	δ	RA	δ	RA	ΔE_Q	δ	RA
295 K												
P2R[a]	20.7	0.07	0.19	15	33.1	0.00	10	−0.10	23	0.57	0.30	41
P5R[b]	20.7	0.02	0.21	16	32.5	0.01	20	−0.13	24	0.56	0.30	33
P7R	20.7	0.04	0.20	22	32.6	0.00	31	−0.13	21	0.57	0.30	26
P10R	20.8	0.04	0.20	24	32.8	0.00	36	−0.12	19	0.57	0.29	21
15 K												
P2R[c]	25.6	−0.05	0.36	19	34.4	0.12	16	−0.01[e]	28	0.55	0.41	27
P5R[d]	25.6	−0.01	0.35	16	34.5	0.12	29	−0.01[e]	27	0.55	0.40	22
P7R	25.8	0.00	0.33	21	34.6	0.12	40	−0.01	24	0.56	0.42	15
P10R	25.7	0.01	0.33	24	34.4	0.12	43	−0.01	23	0.57	0.42	10

a Also present is a weak doublet with ΔE_Q about 1.58 mm/s, $\delta = 0.79$[e] mm/s and RA ~11%.
b Also present is a weak doublet with ΔE_Q about 1.58 mm/s, $\delta = 0.79$[e] mm/s and RA ~7%.
c Also present is a weak doublet with ΔE_Q about 1.52 mm/s, $\delta = 0.89$ mm/s and RA ~10%.
d Also present is a weak doublet with ΔE_Q about 1.53 mm/s, $\delta = 0.81$ mm/s and RA ~6%.
e Fixed parameter value.

FEG–SEM images (Fig. 1a and b) of the powders reveal that they are made up of 2–5 μm grains assembled into tabular-like aggregates. However, the observation of smaller entities and of side-views of the tabular-grains reveals the so-called vermicular microstructure with much looser aggregates made up of 0.2–0.5 μm primary grains or crystallites. The BET specific surface area of these powders is in the range 4.4–6.0 m^2/g, in good agreement with the usual values for corundum. Interestingly, FEG–SEM images (Fig. 1c and d) of the walls of the self-supported foams reveal a much more homogeneous microstructure, with grains generally smaller than 0.5 μm and appearing relatively densely packed. The BET specific surface area of the foams is in the range 10.1–18.7 m^2/g, the increase as compared to the powders probably reflecting the lower average grain size.

3.2. *Composite powders and foams*

Analyses of the XRD patterns (see Supplementary Data, Figure S1) of the PXR powders reveals the pattern of a corundum

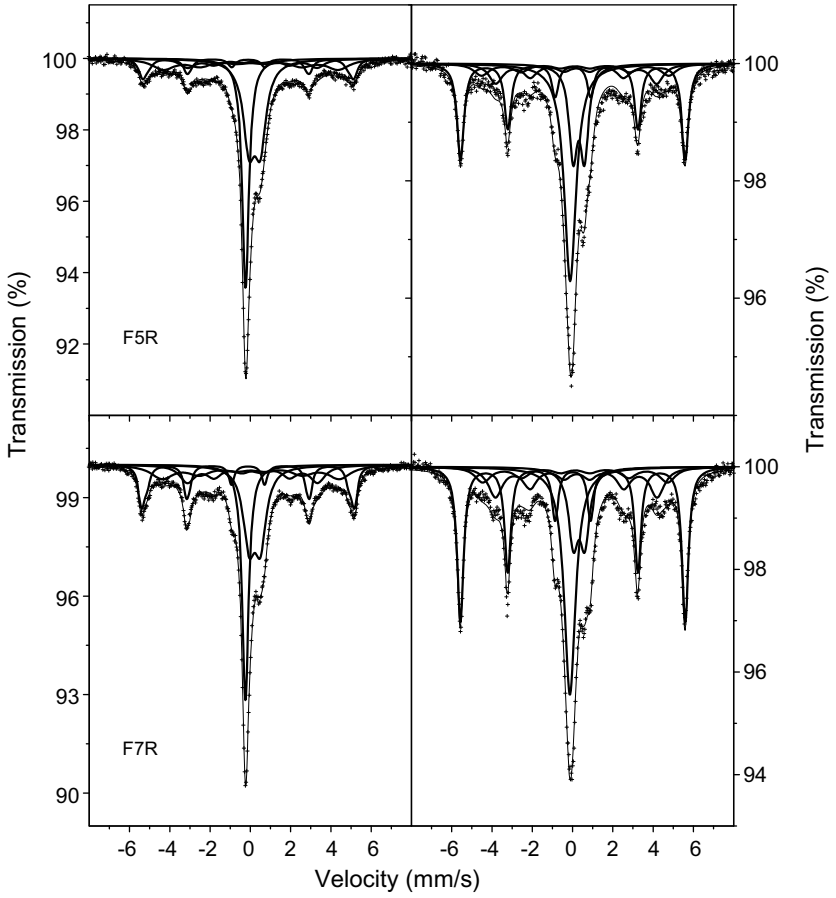

Fig. 3 – MS of the CNTs–Fe–Al_2O_3 foams (F5R and F7R) measured at 295 K (left) and 15 K (right).

Table 3 – Mössbauer results of the CNTs–Fe/alumina foams at 295 K and 15 K. The quadrupole shifts ($2\varepsilon_Q$), quadrupole splitting (ΔE_Q) and isomer shifts (δ) are given in mm/s, the hyperfine fields (B_{hf}) are in T and the relative spectral areas (RA) are given in %. The values of isomer shifts are with reference to metallic iron.

Sample	Fe_3C				α-Fe			γ-Fe–C		$(Al,Fe)_2O_3$			$Fe_{1-y}C_y$		
	B_{hf}	$2\varepsilon_Q$	δ	RA	B_{hf}	δ	RA	δ	RA	ΔE_Q	δ	RA	B_{hf}	δ	RA
295 K															
F2R	20.2[a]	0.03[a]	0.19[a]	8				−0.09	27	0.55	0.32[a]	65			
F5R	19.9	0.03[a]	0.19[a]	10	33.5	0.00	13	−0.13	27	0.56	0.33	33	26.8	0.13[a]	17
F7R	20.0	0.03[a]	0.20	15	33.4	0.00	19	−0.13	23	0.56	0.33	25	27.4	0.13[a]	18
15 K															
F2R	24.8	−0.03[a]	0.31[a]	14	34.6	0.11[a]	10	−0.01[a]	18	0.55	0.42[a]	53	28.8	0.24[a]	5
F5R	24.7	−0.03[a]	0.31[a]	12	34.7	0.12	31	−0.01	31	0.56	0.42	17	29.0	0.24[a]	9
F7R	24.7	−0.03[a]	0.31[a]	16	34.7	0.12	38	−0.02	24	0.57	0.43	13	28.7	0.24[a]	9

a Fixed value.

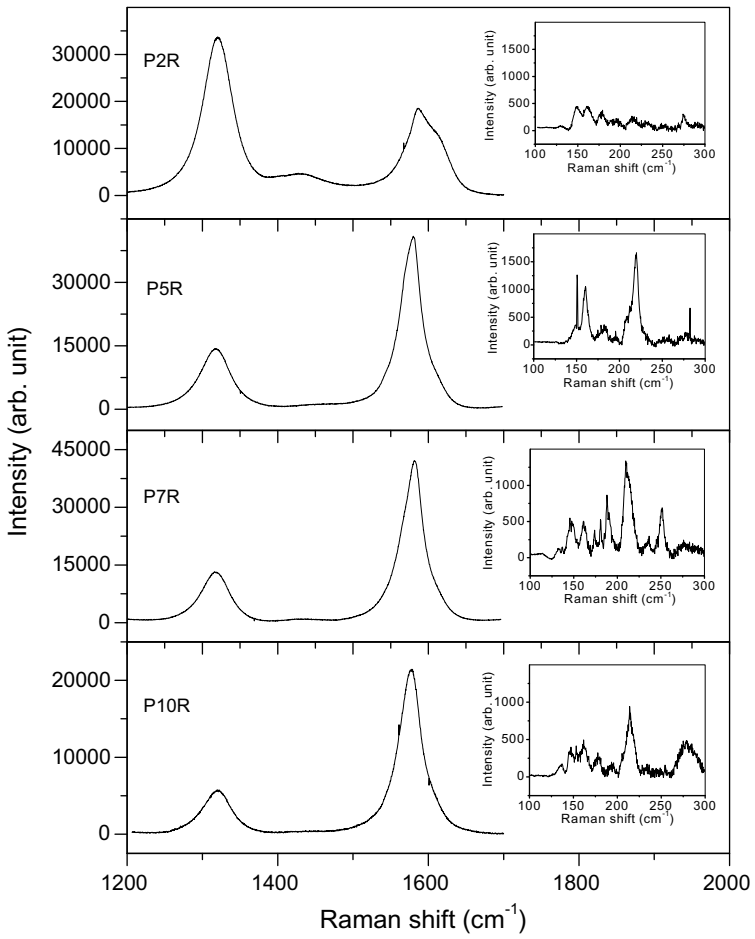

Fig. 4 – High-frequency range of the Raman spectra (632.82 nm) showing the D and G bands for the CNTs–Fe–Al_2O_3 powders and (inset) the corresponding low-frequency range showing the RBM peaks.

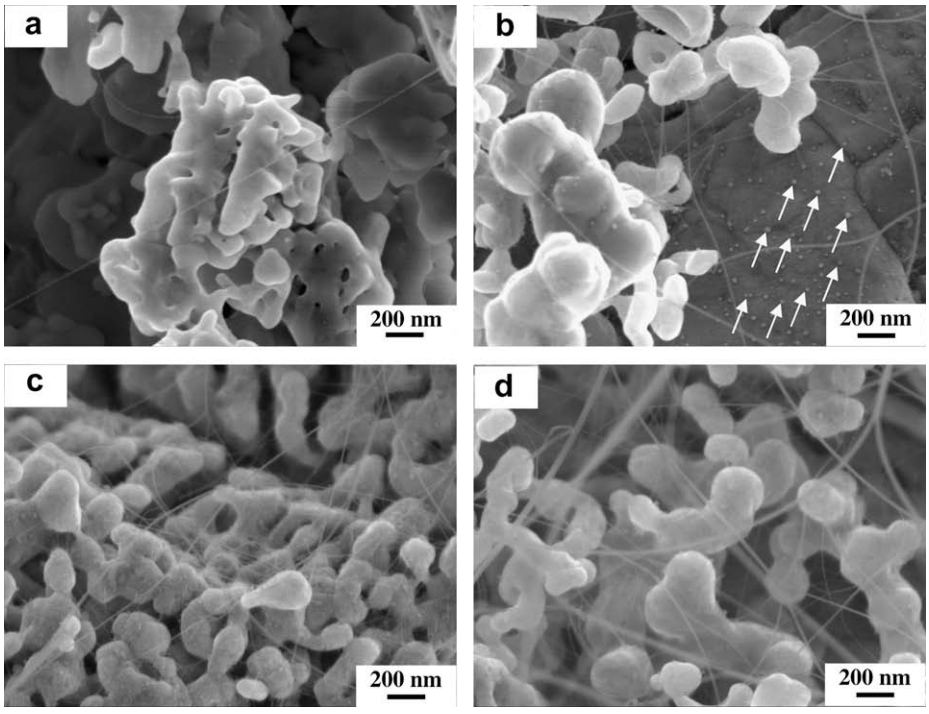

Fig. 5 – FEG–SEM images of the powders: P2R (a), P5R (b), P7R (c) and P10R (d).

phase and the peaks of Fe_3C and α-Fe with increasing intensities upon the increasing iron content. It is difficult to separate the XRD patterns of Fe_3C and α-Fe because the respective main peaks are rather broad and strongly overlapping. γ-Fe may also be present, but cannot be observed because the main γ-Fe peak (d_{111} = 0.208 nm) is masked by the corundum (d_{113} = 0.209 nm) and Fe_3C (d_{121} = 0.210 nm) peaks. As expected, the XRD patterns of the FXR foams (see Supplementary Data, Figure S2) show features essentially similar to those observed for the PXR powders.

The Mössbauer spectra collected at 295 K and 15 K are reproduced in Fig. 2 left and right, respectively. Three of the subspectral components found in the Mössbauer spectra of the parent oxides have vanished: the α-Fe_2O_3 sextet, the weak Fe^{3+} doublet and the singlet due to metallic Fe clusters. Moreover, only part of the main Fe^{3+} doublet has remained, the extent depending on the initial iron concentration, whilst three other components have appeared. Thus, four components were found to be required to obtain adequate fits of these spectra: (i) an outer sextet with hyperfine parameters typical of the α-Fe phase; (ii) an inner sextet that can be attributed to Fe_3C; (iii) a central singlet due to a γ-Fe phase, maybe alloyed with carbon; and (iv) a doublet that can be ascribed to Fe^{3+} species substituting in the Al_2O_3 structure. For samples P2R and P5R, meticulous fitting attempts of their Mössbauer spectra have led to the conclusion that an additional, but weak (⩽11% of total absorption area) and rather ill-defined doublet has to be included in the model. Its quadrupole splitting ΔE_Q was found to be ∼1.6 mm/s and its isomer shift $\delta \approx 0.8$ mm/s at 295 K. This latter value is neither typical of Fe^{3+}, nor of Fe^{2+}, but is rather in between. Moreover, the ΔE_Q value is unusually high for Fe^{3+}. It is proposed that the resolved broad doublet is actually an approximation for the spectrum of a hercynite phase ($FeAl_2O_4$). The Mössbauer spectrum of such spinel-type compounds are composed of several quadrupole doublets arising from Fe^{2+} and from Fe^{3+}, as such rendering their Mössbauer spectrum very complicated and highly unresolved [11–15]. Consequently, when fitting such a composition of Fe^{2+} and Fe^{3+} doublets by one single doublet, one obtains a broad line width and hyperfine parameters with values that are intermediate between those characteristic for Fe^{2+} and Fe^{3+}, respectively.

The relevant numerical data resulting from the adjustments of the respective spectra are listed in Table 2. The relative spectral areas (RA) of the various components (Table 2), change significantly when the temperature is lowered from 295 K to 15 K. This can be due either to superparamagnetic effects in some of the constituents at 295 K, or to the weaker resolution of the respective subspectra, making the derived Mössbauer parameters, in particular the RA values, less reliable. The occurrence of superparamagnetism is a well-known property of magnetic small particles ([16] and references therein). In the Mössbauer spectra, this phenomenom is reflected in the collapse of the magnetically split spectrum into an apparently paramagnetic doublet or singlet at temperatures lower than the respective Curie or Néel point of the involved material in bulk appearance. This collapse is due to fast relaxation of the magnetization vector as a whole. It is reasonable to consider that the Fe phases present in the composites exhibit relatively broad particle-size distributions. Consequently, some of these phases may present a superparamagnetic effect at relatively high temperatures, resulting in the appearance of a quadrupole doublet or a singlet in the Mössbauer spectra acquired at these temperatures. In view of this feature it could be that part of the Fe^{3+} doublet and/or the singlet presently observed at the higher temperature (295 K) is actually due to Fe constituents that at 15 K are experienced as being magnetic, i.e., as a sextet. In this sense, one may raise doubts about the validity of the Mössbauer parameters obtained for the Mössbauer spectra at 295 K, in particular the relative spectral areas RA. For this reason, only the data referring to 15 K are thought to be reliable and useful. The main differences between the four powders concern the RA values for the $(Al,Fe)_2O_3$ doublet and the α-Fe sextet. The RA value for the $(Al,Fe)_2O_3$ doublet steadily decreases from P2R to P10R,

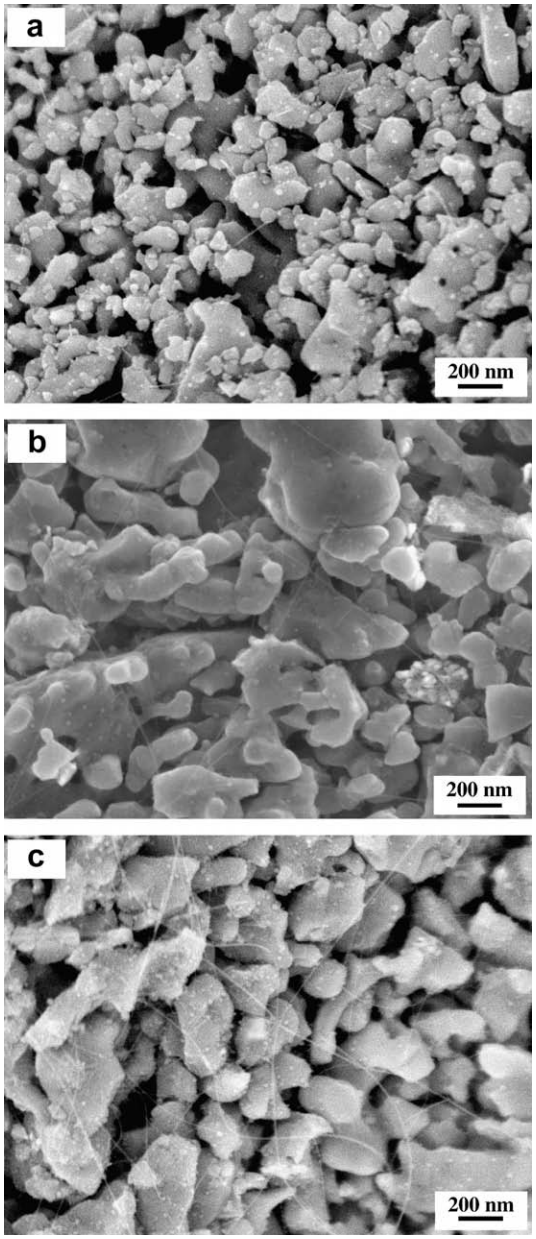

Fig. 6 – FEG–SEM images of the foams: F2R (a), F5R (b) and F7R (c).

showing that the reduction is comparatively easier when the total iron content is increased. The α-Fe sextet is significantly more abundant for P7R and P10R than for P2R and P5R, which could be a consequence of the easier reduction process and could also reflect the presence of a hematite-rich phase (Table 1) in the corresponding P7 and P10 powders.

Typical Mössbauer spectra recorded at 295 K and 15 K for the FXR foams are reproduced in Fig. 3 and the relevant Mössbauer parameters are reported in Table 3. Some constraints had to be imposed to the fit procedure. They are indicated in the footnotes to Table 3. In the applied fitting model, generally five patterns were included: the four components (corresponding to α-Fe, Fe_3C, γ-Fe-C and Fe^{3+}) that were also present in the Mössbauer spectra of the PXR powders, and an additional sextet. This later component is possibly due to an $Fe_{1-y}C_y$ alloy [17]. However, this fifth component could not be resolved from the 295 K spectrum for F2R, and also the α-Fe subspectrum was not detected in this latter spectrum. Note that the relative abundance of the $(Al,Fe)_2O_3$ doublet for F2R (53%) is much higher than for P2R (27%), indicating that the reduction was significantly more difficult for the former specimen. The *RA* values for F5R and F7R are similar to those for P5R and P7R. These results reveal that contrary to some expectations, the lower grain size and higher specific surface area of the starting oxide foams do not lead to an easier reduction and thus to the formation of

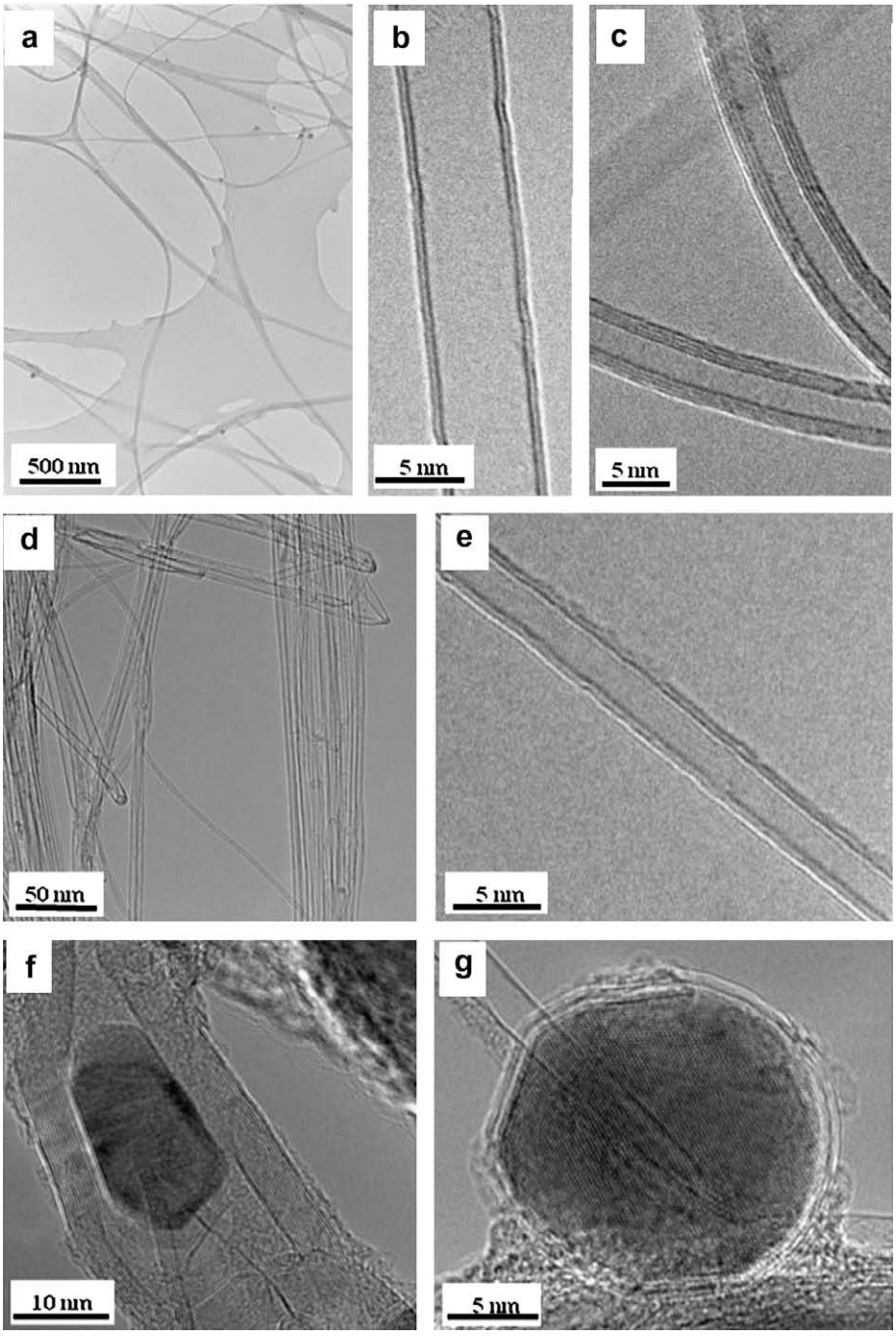

Fig. 7 – HRTEM images for powder P5R.

more α-Fe, Fe_3C and/or γ-Fe-C potentially active particles for the formation of CNTs. This could be due to the higher packing of the solid solution grains in the walls of the foam.

The carbon content (C_n) was found equal to 0.6, 1.0, 1.9 and 3.3 wt% for P2R, P5R, P7R and P10R, respectively. This evolution is in agreement with earlier results [18] obtained with powders by the oxalate (not oxinate) route, although the values are lower. This difference arises because in the earlier study [18], there was a dwell time of 4 h at the maximum reduction temperature, whereas no dwell time was applied for the present study. The carbon content was found equal to 0.8, 1.4 and 1.5 wt% for F2R, F5R and F7R, respectively. These values are not much different than those measured for the PXR powders, which is in line with the conclusion of the above Mössbauer spectroscopic study.

The high-frequency range (1200–1800 cm^{-1}) of the Raman spectra (Fig. 4) shows the D band (ca. 1320 cm^{-1}) and the G band (ca. 1580 cm^{-1}). The ratio between the intensity of the D band and the G band, $I_{D/G}$ is very high for P2R (180%) and much lower (close to 30%) for the other three powders. An increasing $I_{D/G}$ value corresponds to a higher proportion of sp^3-like carbon, which is generally attributed to the presence of more structural defects. In addition, the G band for P2R shows a shoulder at higher frequency (ca. 1615 cm^{-1}), which is typical of defective graphite-like materials [19]. The presence of radial-breathing-modes (RBM) peaks in the low-frequency range (100–300 cm^{-1}) of the spectrum (insets in Fig. 4), the frequencies of which are inversely proportional to the CNT diameters, is usually the sign of the presence of small-diameter CNTs, such as SWCNTS and DWCNTs. Only very weak RBM peaks are observed for P2R. Note however that the Raman process is influenced by optical resonance and it is thus impossible to detect all present CNTs using only one wavelength. Moreover, the peak intensities do not reflect the real amount of individual CNTs because of the resonance effect which amplifies the Raman signal from certain CNT. The Raman spectra (see Supplementary Data, Figure S3) of the FXR composite foams clearly reveal a decrease in the intensity ratio $I_{D/G}$ with increasing Fe content (88, 66 and 33% for F2R, F5R and F7R, respectively). Compared to the corresponding PXR powders, the $I_{D/G}$ values are much lower, higher and similar for F2R, F5R and F7R, respectively. RBM peaks are detected for all three composite foams.

FEG–SEM images (Fig. 5) of the PXR specimens reveal the presence of long, flexible filaments, with a smooth and regular surface, on the surface of the oxide grains and bridging several grains. The quantity of such filaments increases with increasing X. All filaments have a diameter smaller than 30 nm and a length of the order of some tens of micrometers. From earlier results, it is known that such filaments are isolated CNTs and/or CNTs bundles. Spherical particles 5–20 nm in diameter that may be α-Fe, Fe_3C and/or γ-Fe–C (some of which are arrowed on Fig. 5b) are observed at the surface of the alumina grains. Most of these particles do not appear to be connected to a CNT, indicating that they have been inactive for the formation of CNT. It is interesting to note that the presence of undesirable thick, short carbon nanofibers is not observed. FEG–SEM images (Fig. 6) of the FXR specimens reveal features essentially similar to what is observed for the PXR samples.

Typical HRTEM images collected for sample P5R are shown in Fig. 7. The images show CNT bundles (Fig. 7a and d), DWCNTs (Fig. 7b and e) and CNTs with four walls (Fig. 7c). Carbon nanofibers partly filled with a metal particle (Fig. 7f) are very rarely observed, in agreement with the FEG–SEM results. An inactive particle (α-Fe, Fe_3C or γ-Fe–C) covered by several graphene layers is shown in Fig. 7g. Fig. 8 presents histograms of the number of walls and diameter distributions, which were obtained by measuring CNTs on similar HRTEM images for sample P5R. The distribution of the number of walls (Fig. 8a) shows that about 65% of CNTs are DWCNTs. Most of the other CNTs have three, four or five walls, the SWCNTs accounting only for less than 5%. The diameter distribution (Fig. 8b) spans a relatively broad range. The inner diameter averages at ~2.7 nm and the outer diameter at ~4.4 nm. HRTEM images (Fig. 9) were collected for sample F5R. Note that the poorly-ordered carbon observed at the surface of the CNTs originates from CNTs damaging under the electron beam. The important difference compared to P5R is that SWCNTs (Fig. 9a and b) and DWCNTs (Fig. 9c) appear to be considerably more abundant for F5R, to the detriment of MWCNTs. Indeed, the histogram of the number of wall indicates 60% SWCNTs and 40% DWCNTs (see Supplementary Data, Figure S4). This finding is in agreement with previous results [7,8] showing that the selectivity of the method towards SWCNTs is much higher when the starting material is in the form of a foam as opposed to a powder. The XRD and Mössbauer spectroscopic studies do not seem to reveal differences

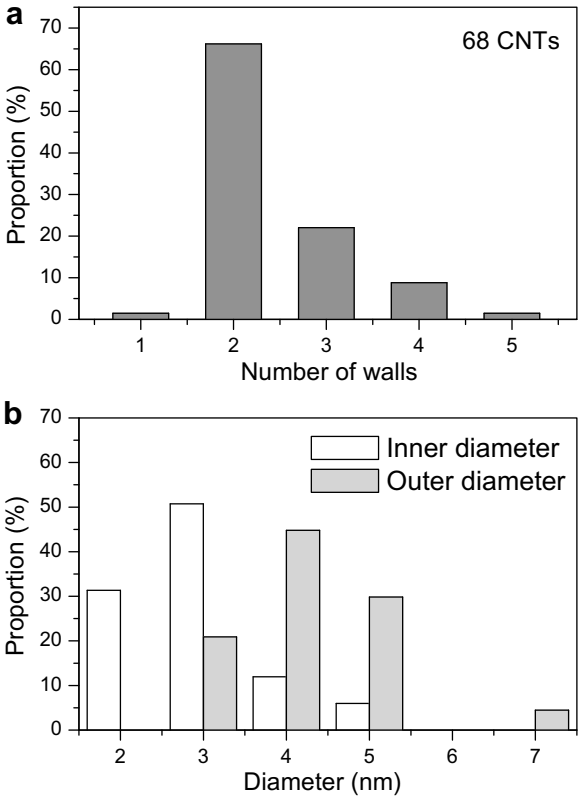

Fig. 8 – Number of walls (a) and CNT diameter (b) distributions evaluated from the HRTEM images for powder P5R.

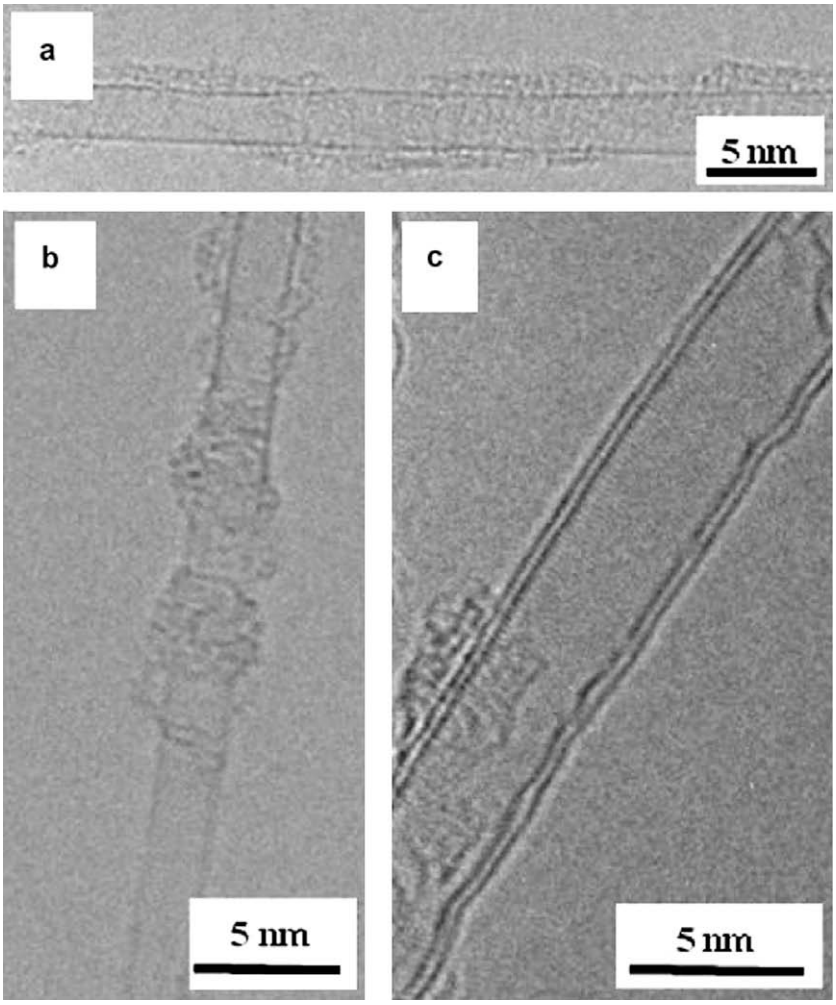

Fig. 9 – HRTEM images for foam F5R.

that could account for this, prompting out the need for future studies.

4. Conclusions

The Mössbauer spectroscopy technique revealed that four components (corresponding to α-Fe, Fe_3C, γ-Fe–C and Fe^{3+}) were present in the Mössbauer spectra of the composite powders, and that an additional sextet, possibly due to an $Fe_{1-y}C_y$ alloy, is also present in the spectra of the composite foams. Contrary to some expectations, the lower grain size and higher specific surface area of the starting oxide foams compared to the powders do not lead to an easier reduction and thus to the formation of more α-Fe, Fe_3C and/ or γ-Fe–C potentially active particles for the formation of CNTs. This could be due to the higher packing of the solid solution grains in the walls of the foam. Thus, there is no gain in the quantity of CNTs, but HRTEM images interestingly revealed that the selectivity of the method towards SWCNTs is much higher when the starting material is in the form of foam (60% SWCNTs and 40% DWCNTs) as opposed to a powder (5% SWCNTs, 65% DWCNTs and 30% MWCNTs).

Acknowledgements

This work was partially funded by the Fund for Scientific Research – Flanders, and by the Special Research Fund (BOF, Bijzonder Onderzoeksfonds), UGent (B/06633), Belgium. The authors would like to thank Mr. Lucien Datas for assistance in HRTEM observations. All electron microscopy observations were performed at TEMSCAN, the "Service Commun de Microscopie Electronique à Transmission", Université Paul Sabatier, Toulouse.

Appendix A. Supplementary data

Supplementary data associated with this article can be found, in the online version, at doi:10.1016/j.carbon.2008.10.027.

REFERENCES

[1] Loiseau A, Blase X, Charlier J-C, Gadelle P, Journet C, Laurent Ch, et al. In: Loiseau A, Launois P, Petit P,

Roche S, Salvetat JP, editors. Understanding carbon nanotubes: from basics to applications. Berlin: Springer. p. 49–130.
[2] Hafner JH, Bronikowski MJ, Azamian BK, Nikolaev P, Rinzler AG, Colbert DT, et al. Catalytic growth of single-wall carbon nanotubes from metal particles. Chem Phys Lett 1998;296:195–202.
[3] Peigney A, Coquay P, Flahaut E, Vandenberghe RE, De Grave E, Laurent Ch. A study of the formation of single- and double-walled carbon nanotubes by a CVD method. J Phys Chem B 2001;105:9699–710.
[4] Peigney A, Laurent Ch, Dobigeon F, Rousset A. Carbon nanotubes grown in situ by a novel catalytic method. J Mater Res 1997;12:613–5.
[5] Laurent Ch, Peigney A, Flahaut E, Rousset A. Synthesis of carbon nanotubes-Fe–Al_2O_3 powders. Influence of the characteristics of the starting $Al_{1.8}Fe_{0.2}O_3$ oxide solid solution. Mater Res Bull 2000;35:661–73.
[6] Laurent Ch, Peigney A, Rousset A. Synthesis of carbon nanotubes-Fe–Al_2O_3 nanocomposites powders by selective reduction of different $Al_{1.8}Fe_{0.2}O_3$ solid solutions. J Mater Chem 1998;8(5):1263–72.
[7] Rul S, Laurent Ch, Peigney A, Rousset A. Carbon nanotubes prepared in situ in a cellular ceramic by the gelcasting-foam method. J Eur Ceram Soc 2003;23:1233–41.
[8] Cordier A, Flahaut E, Viazzi C, Laurent Ch, Peigney A. In situ CCVD synthesis of carbon nanotubes within a commercial ceramic foam. J Mater Chem 2005;15:4041–50.
[9] De Resende VG, Cordier A, De Grave E, Laurent Ch, Eeckhout SG, Giuli G, et al. Presence of metallic Fe nanoclusters in α-$(Al,Fe)_2O_3$ solid solutions. J Phys Chem C 2008;112:16256–63.
[10] Vandenberghe RE, De Grave E, de Bakker PMA. On the methodology of the analysis of Mössbauer spectra. Hyperfine Interact 1994;83:29–49.
[11] Rossiter MJ. The Mössbauer spectra of some spinel oxides containing iron. J Phys Chem Solids 1965;26:775–9.
[12] Ôno K, Ito A, Syono Y. Mössbauer study of Fe^{2+} in some normal spinels. Phys Lett 1965;19:620–1.
[13] Yagnik CM, Mathur HB. A Mössbauer and X-ray diffraction study on the cation distribution in $FeAl_2O_4$. J Phys C 1968;1:469–72.
[14] Larsson L, O'Neill HSTC, Annersten H. Crystal chemistry of synthetic hercynite ($FeAl_2O_4$) from XRD structural refinements and Mössbauer spectroscopy. Eur J Mineral 1994;6:39–51.
[15] Andreozzi GB, Baldi G, Bernardini GP, Di Benedetto F, Romanelli M. ^{57}Fe Mössbauer and electronic spectroscopy study on a new synthetic hercynite-based pigment. J Eur Ceram Soc 2004;24:821–4.
[16] Long GJ. Mössbauer spectroscopy applied to inorganic chemistry. New York: Plenum Press; 1987. p. 91–93.
[17] De Resende VG, Cordier A, De Grave E, Weibel A, Peigney A, da Costa GM, et al. Synthesis of γ-$(Al_{1-x}Fe_x)_2O_3$ solid solutions from oxinate precursors and formation of carbon nanotubes from the solid solutions using methane or ethylene as carbon source. J Mater Res 2008;23:3096–111.
[18] Peigney A, Laurent Ch, Dumortier O, Rousset A. Carbon nanotubes–Fe–alumina nanocomposites. Part I: influence of the Fe content on the synthesis of powders. J Eur Ceram Soc 1998;18:1995–2004.
[19] Jorio A, Pimenta MA, Souza Filho AG, Saito R, Dresselhaus G, Dresselhaus MS. Characterizing carbon nanotube samples with resonance Raman scattering. New J Phys 2003;5:139.1–139.17.